AIAA 2001-2574

Towards Optimal Multigrid Efficiency for the Navier-Stokes Equations

R. C. Swanson
NASA Langley Research Center
Hampton, VA 23681

15th Computational Fluid Dynamics Conference
June 11–June 14, 2001
Anaheim, CA

TOWARDS OPTIMAL MULTIGRID EFFICIENCY FOR THE NAVIER-STOKES EQUATIONS

R. C. Swanson*
NASA Langley Research Center
Hampton, VA

Abstract

A fast multigrid solver for the steady incompressible Navier-Stokes equations is presented. Unlike time-marching schemes, this approach uses relaxation of the steady equations. Application of this method results in a discretization that correctly distinguishes between the advection and elliptic parts of the operator, allowing efficient smoothers to be constructed. Numerical solutions are shown for flow over a flat plate and a Kármán-Trefftz airfoil. Using collective Gauss-Seidel line relaxation in both the vertical and horizontal directions, multigrid convergence behavior approaching that of $O(N)$ methods is achieved. The computational efficiency of the numerical scheme is compared with that of a Runge-Kutta based multigrid method.

Introduction

One of the critical needs in computational fluid dynamics is faster flow solvers. Multigrid is a well known method of convergence acceleration that is widely used in Euler and Reynolds-averaged Navier-Stokes codes. These applications of multigrid generally are based on the unsteady equations using some temporal integrator as the smoother, combined with a full-approximation scheme (FAS) multigrid iteration. A common approach is one originally proposed by Jameson.[1] Starting with the unsteady equations, a finite-volume spatial discretization with explicit artificial viscosity is combined with a Runge-Kutta (R-K) time integration as a smoother. An alternative approach[2–4] is to use upwind-differencing and implicit time integration as the smoother. However, these approaches have resulted in poor multigrid efficiency. When applied to high Reynolds number flows over complex geometries, convergence rates are often worse than 0.99. There is clearly a need to develop substantially more efficient multigrid solvers.

According to Brandt,[5] one of the major obstacles to achieving better multigrid performance for advection dominated flows is that the coarse grid provides only a fraction of the needed correction for smooth error components. This obstacle can be removed by designing a solver that effectively distinguishes between the elliptic, parabolic, and hyperbolic (advection) factors of the system and treats each one appropriately. For instance, advection can be treated by space marching, while elliptic factors can be treated by multigrid. The efficiency of such an algorithm will be essentially identical to that of the solver for the elliptic factor only, and thereby attain so-called "textbook" multigrid efficiency.

Relatively little research has been done in the area of multigrid algorithms for the Navier-Stokes equations based upon factorizable discrete schemes. Brandt[5] has presented an approach called "distributive relaxation" by which one can construct smoothers that effectively distinguish between the different factors of the operator. Using this approach, Brandt and Yavneh have demonstrated textbook multigrid efficiency for the incompressible Navier-Stokes equations.[6] Their results are for a simple geometry and a Cartesian grid, using a staggered-grid discretization of the equations.

Recently, Thomas, Diskin, and Brandt[7] achieved textbook multigrid efficiency for high Reynolds number incompressible wake and boundary layer flows associated with a flat plate. Their scheme uses a staggered grid approach with distributed relaxation and defect correction. With the distributive relaxation the system of equations was decomposed (i.e., factorized) everywhere, except near boundaries where they remained coupled. In all calculations Cartesian grids were used.

Sidilkover and Asher[11] introduced a fast multigrid solver for the incompressible Navier-Stokes equations that does not require a staggered grid arrangement of flow variables. With a pressure Poisson formulation as a foundation, a factorizable discrete scheme is derived. In this work also only simple model problems were solved using uniform Cartesian grids.

In this paper, an alternative to distributive relaxation is presented. It is a generalization of the approach of Sidilkover and Ascher[11] and a continuation of the work of Roberts and Swanson.[10] This approach can be classified as a method of the Weighted Gauss-Seidel type.[5] A conventional vertex-based finite-volume or finite-difference discretization of the primitive variables is used, avoiding the need for staggered grids. This simplifies the restriction and prolongation operations, because the same operator can be used for all variables. A projection operator is applied to the system of equations, resulting in a Poisson equation for the pressure. In the case of the incompressible Navier-Stokes equations the physical diffusion terms in the pressure equation require approximation only at boundaries. A suitable boundary condition for general geometries can be derived. The Poisson equation for the pressure may be treated by Gauss-Seidel relaxation, while the advection terms of the momentum equation are treated by space-marching. Because the elliptic and advection parts of the system are decoupled, ideal multigrid efficiency is possible. With the present scheme line relaxation is used to treat

* Research Scientist

the anisotropy of mesh aspect ratio that generally occurs in resolving viscous flows.

Mathematical Formulation

The incompressible Navier-Stokes equations in primitive variables are

$$\begin{aligned} uu_x + vu_y + p_x &= \nu(u_{xx} + u_{yy}), \\ uv_x + vv_y + p_y &= \nu(v_{xx} + v_{yy}), \\ u_x + v_y &= 0, \end{aligned}$$

where u and v are the components of the velocity in the x and y directions, respectively, p is the pressure, and the subscripts denote partial differentiation. The density is taken to be one. The advection-diffusion operator is defined by

$$Q_\nu \equiv Q - \nu\Delta, \tag{1}$$

where $Q = u\partial_x + v\partial_y$, Δ is the Laplacian operator, and ∂_x, ∂_y are the partial differentiation operators. The coefficient ν is the reciprocal of the Reynolds number, $\nu = 1/Re$. The incompressible Navier-Stokes equations may be written as

$$\mathbf{Lq} = \begin{pmatrix} Q_\nu & 0 & \partial_x \\ 0 & Q_\nu & \partial_y \\ \partial_x & \partial_y & 0 \end{pmatrix} \begin{pmatrix} u \\ v \\ p \end{pmatrix} = 0. \tag{2}$$

Introducing the adjoint to Q, defined by

$$Q^*_\nu(f) \equiv -\partial_x(uf) - \partial_y(vf) + \Delta(\nu f), \tag{3}$$

a projection operator $\mathbf{P}$ is defined:

$$\mathbf{P} = \begin{pmatrix} I & 0 & 0 \\ 0 & I & 0 \\ \partial_x & \partial_y & Q^*_\nu \end{pmatrix}. \tag{4}$$

Applying the projection operator to the Navier-Stokes equations yields

$$\tilde{\mathbf{L}}\mathbf{q} \equiv \mathbf{PLq} = \begin{pmatrix} Q_\nu & 0 & \partial_x \\ 0 & Q_\nu & \partial_y \\ 0 & 0 & \Delta \end{pmatrix} \begin{pmatrix} u \\ v \\ p \end{pmatrix} + \text{s.p.t.}, \tag{5}$$

The matrix operator on the right-hand side consists of the principal part of $\tilde{\mathbf{L}}$, and "s.p.t." are the subprincipal terms, in the terminology of Brandt.[5] These terms arise because the coefficients u and v in the operators Q_ν and Q^*_ν are not constant. It is important to note that the subprincipal terms can be ignored for the purpose of constructing a relaxation scheme.

The operator on the left-hand side of Eq. (5) is upper triangular. The pressure satisfies a Poisson equation for which a conventional relaxation method, such as Gauss-Seidel, can be applied. Upwind differencing of the advection operator in the momentum equations allows downstream relaxation to be used. The strategy used to relax the system is to first update the pressure. The pressure update contributes to the velocity update through the gradient terms in the right-hand column of the operator in Eq. (5). Finally, the velocity components are updated by relaxing in the streamwise direction.

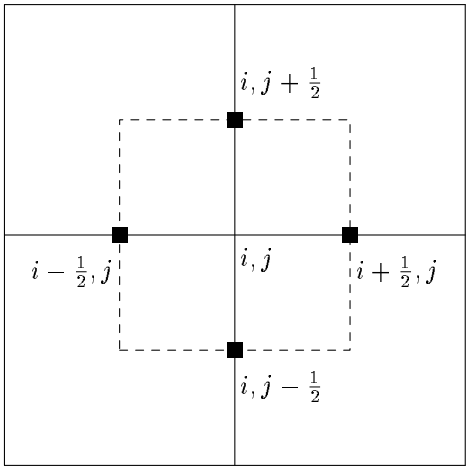

Fig. 1 Primary and dual cells on quadrilateral grid.

Discretization

The first step in approximating $\tilde{\mathbf{L}}$ is to discretize the Navier-Stokes equations (2). Consider a typical grid vertex as shown in Fig. 1. The momentum equations are discretized using a second-order accurate upwind difference stencil for the advection part of operator (1), and central differencing for the physical diffusion contribution. Central differencing is also used for the pressure gradient term.

Consider the discretization of the term $u\partial_x u$ in the x-momentum equation, assuming a Cartesian grid for simplicity. The second-order upwind-difference discretization of this term may be written as

$$u\partial^h_x u|_{SO} = \frac{3}{2h}u_{i-1/2,j}(u_{i,j} - u_{i-1,j}) - \frac{1}{2h}u_{i-3/2,j}(u_{i-1,j} - u_{i-2,j}) \tag{6a}$$

when $u > 0$, and

$$u\partial^h_x u|_{SO} = \frac{3}{2h}u_{i+1/2,j}(u_{i+1,j} - u_{i,j}) - \frac{1}{2h}u_{i+3/2,j}(u_{i+2,j} - u_{i+1,j}) \tag{6b}$$

when $u < 0$. Here, the superscript h denotes the discrete approximation to the corresponding differential operator, and the average velocity components $u_{i\pm1/2,j}$ are

$$\begin{aligned} u_{i+1/2,j} &= \frac{1}{2}(u_{i+1,j} + u_{i,j}), \\ u_{i-1/2,j} &= \frac{1}{2}(u_{i,j} + u_{i-1,j}). \end{aligned}$$

Analogous expressions may be written for the $v\partial^h_y$ operator.

The projection operator $\mathbf{P}$ is applied to the discrete equations to obtain the residual for the pressure Poisson equation of Eq. (5). Letting $R_{p_{ij}}$ be the pressure equation residual at vertex (i, j), the application of $\mathbf{P}$ can be written

in integral form,

$$R_{p_{ij}} = \oint_{\partial A_{ij}} \left(\boxed{Q_\nu^h u + \partial_x^h p} - u \boxed{\left(\partial_x^h u + \partial_y^h v \right)} \right) dy - \left(\boxed{Q_\nu^h v + \partial_y^h p} - v \boxed{\left(\partial_x^h u + \partial_y^h v \right)} \right) dx, \quad (7)$$

where A_{ij} is the area of the control volume centered on vertex (i,j). This control volume is the area bounded by the dual grid cell, shown as the dashed lines in Fig. 1. The discretization of the pressure equation is done by first discretizing the boxed terms of Eq. (7) on the edges of the dual grid cell. The evaluation points are shown as solid squares. To evaluate the gradient of pressure p at the dual grid face $(i-1/2, j)$ the partial derivatives are written as

$$p_x = p_\xi \xi_x + p_\eta \eta_x, \qquad p_y = p_\xi \xi_y + p_\eta \eta_y, \quad (8)$$

where ξ and η are the generalized coordinates corresponding to the i and j directions on the grid respectively. The derivatives $\partial_\xi p$ and $\partial_\eta p$ are approximated at the face center by

$$\begin{aligned} \partial_\xi^h p\Big|_{i-1/2,j} &= p_{i,j} - p_{i-1,j}, \\ \partial_\eta^h p\Big|_{i-1/2,j} &= \frac{1}{4}\left(p_{i,j+1} + p_{i-1,j+1} - p_{i,j-1} - p_{i-1,j-1} \right), \end{aligned} \quad (9)$$

with similar expressions for the faces $(i+1/2, j)$, $(i, j+1/2)$, and $(i, j-1/2)$. The gradients of u and v are found the same way. The grid metric terms ξ_x, ξ_y, η_x, and η_y are also evaluated on the dual grid face centers. These expressions are used in the boxed terms in Eq. (7). The integral (7) is then evaluated to get the pressure equation residual at the vertex (i,j), taking the boxed terms to be constant over each face of the dual grid cell. For a uniform Cartesian grid, the principal part of the resulting stencil is a conventional five-point approximation to the Laplacian operating on the pressure.

With the velocity gradients known at the faces of the dual grid cell of Fig. 1, one can easily determine the physical viscous terms in the momentum equations. By applying Green's theorem, as in Eq. (7), to the dual grid cell, the Laplacian in Δu and Δv is approximated by

$$\begin{aligned} \Delta u &= \oint_{\partial A_{ij}} (u_x dy - u_y dx), \\ \Delta v &= \oint_{\partial A_{ij}} (v_x dy - v_y dx), \end{aligned} \quad (10)$$

Viscous terms also appear in the pressure equation, which can be written as

$$\Delta p = -\partial_x[u u_x + v u_y)] - \partial_y[u v_x + v v_y)] + \nu[\partial_x(\Delta u) + \partial_y(\Delta v)], \quad (11)$$

where the terms on the right side of (11) are subprincipal terms with respect to relaxation. If the functions $u(x,y)$ and $v(x,y)$, as well as their spatial derivatives, are continuous, then the order of differentiation does not matter. Consider a two-dimensional flow domain where these functions and their derivatives are continuous. Then, in the interior of the domain, the derivatives of the viscous contributions cancel with the application of the continuity equation.

At a solid boundary the viscous terms do not cancel. The inviscid subprincipal terms of Eq. (11) vanish when the no-slip conditions are applied, as in viscous flows. The pressure equation reduces to

$$\Delta p = \nu[\partial_x(\Delta u) + \partial_y(\Delta v)], \quad (12)$$

In the discrete problem (12) is approximated for a half dual cell at the boundary. From the momentum equations,

$$\begin{aligned} p_x|_{i,1} &= \nu(\Delta u)_{i,1}, \\ p_y|_{i,1} &= \nu(\Delta v)_{i,1}, \end{aligned} \quad (13)$$

where $j = 1$ corresponds to the surface boundary. The discrete form of Eq. (12) provides the necessary boundary condition for pressure. The present approach for treating the viscous terms in the pressure equation is similar to that of Sidilkover and Asher.[11]

Solution Procedure

Rather than discretizing Eq. (5) directly, the first step of numerical solution procedure is to discretize Eq. (2). The relaxation scheme is constructed by applying the projection operator $\mathbf{P}$ at the discrete level rather than the differential level. A sequence of grids $G_K, G_{K-1}, \ldots, G_0$ is used, where G_K is the finest and G_0 the coarsest. Let $\tilde{\mathbf{L}}_k$ be the discrete approximation to the operator $\tilde{\mathbf{L}}$ and $\mathbf{q}_k$ be the solution on the k-th grid. This system has the form $\tilde{\mathbf{L}}_k \mathbf{q}_k = \mathbf{f}_k$, where the entries of $\tilde{\mathbf{L}}_k$ are 3×3 block matrices which operate on the unknowns $(u, v, p)^T$ at each grid vertex. A general iteration scheme is constructed by writing the operator $\tilde{\mathbf{L}}_k$ as $\tilde{\mathbf{L}}_k = \mathbf{M}_k - \mathbf{N}_k$, where the splitting is chosen such that $\mathbf{M}_k$ is easily inverted. Lexicographic Gauss-Seidel is obtained by taking $\mathbf{M}_k$ to be the block lower-triangular matrix resulting from ignoring the blocks above the diagonal of $\tilde{\mathbf{L}}_k$. A further simplification is obtained if the diagonal blocks of $\mathbf{M}_k$ contain only those entries corresponding to the principal part of the operator. Because the operator in Eq. (5) is upper triangular, the diagonal blocks will then be 3×3 upper triangular matrices.

Letting $\mathbf{q}_k^n$ be the n-th iterate of the solution, the iteration is

$$\mathbf{M}_k \mathbf{q}_k^{n+1} = \mathbf{f}_k + \mathbf{N}_k \mathbf{q}_k^n.$$

Because the operator $\tilde{\mathbf{L}}_k$ is nonlinear, $\mathbf{M}_k$ and $\mathbf{N}_k$ will be functions of $\mathbf{q}_k^n$ and $\mathbf{q}_k^{n+1}$. Letting $\delta \mathbf{q}_k^n \equiv \mathbf{q}_k^{n+1} - \mathbf{q}_k^n$, the iteration may be rewritten as

$$\mathbf{M}_k \delta \mathbf{q}_k^n = \mathbf{f}_k - \tilde{\mathbf{L}}_k \mathbf{q}_k^n. \quad (14)$$

Because $\mathbf{M}_k$ is block lower-triangular, $\delta \mathbf{q}_k^n$ is found by forward substitution and inverting a 3×3 diagonal block at each vertex. The diagonal blocks are upper triangular and are easily inverted.

If upwind differences are used for the advection operator (1) and the grid points are ordered in the flow direction, then the 3×3 blocks of $\mathbf{N}_k$ will have zeroes in the first two rows. In this case, lexicographic Gauss-Seidel relaxation is equivalent to space-marching of the advection terms. The advected error is effectively eliminated in one relaxation

sweep and the convergence rate becomes that of the Poisson equation for the pressure. It is possible to get ideal multigrid convergence rates for the system because each component of the error is treated appropriately.

In the application of line Gauss-Seidel relaxation the unknowns along a given grid line are determined simultaneously. A scalar tridiagonal matrix inversion is required for the pressure equation. Due to the second-order discretization of the advection terms, a scalar pentadiagonal matrix inversion is necessary for the momentum equations.

A straightforward FAS multigrid iteration is applied to the system of equations. Let $\tilde{\mathbf{L}}_{k-1}$ be the coarse grid operator, I_{k-1}^{k} be the fine-to-coarse grid restriction operator, and I_{k}^{k-1} be the coarse-to-fine grid prolongation operator. If $\hat{\mathbf{q}}_k$ is the current solution on grid k, the residual on this grid is $\mathbf{r}_k \equiv \mathbf{f}_k - \tilde{\mathbf{L}}_k \hat{\mathbf{q}}_k$. This leads to the coarse-grid equation

$$\tilde{\mathbf{L}}_{k-1}\mathbf{q}_{k-1} = \mathbf{f}_{k-1} = I_{k-1}^{k}\mathbf{r}_k + \tilde{\mathbf{L}}_{k-1}\left(I_{k-1}^{k}\hat{\mathbf{q}}_k\right). \qquad (15)$$

After solving the coarse-grid equation for $\mathbf{q}_{k-1}$, the fine-grid solution is corrected by

$$\mathbf{q}_k \leftarrow \hat{\mathbf{q}}_k + I_{k}^{k-1}\left(\mathbf{q}_{k-1} - I_{k-1}^{k}\hat{\mathbf{q}}_k\right). \qquad (16)$$

Equation (15) is solved by applying the same relaxation procedure that is used to solve the fine-grid equation. Multigrid is applied recursively to the coarse-grid equation. On the coarsest grid, many relaxation sweeps are performed to insure that the equation is solved completely. A conventional W–cycle is used.

Results

The numerical scheme described in the previous sections has been applied to two incompressible, viscous flow problems. As an initial evaluation of the scheme, high Reynolds number flow past a flat plate is considered. For the second problem flow past a symmetric Kármán-Trefftz airfoil is solved on two different mesh topologies.

The computational domain for the flat plate simulation is displayed in Fig. 2. The inflow boundary ($x = 0$), outflow boundary ($x = 3$), and the upper boundary ($y = 1$) are located one plate length away from the plate. At the inflow boundary, the free-stream conditions ($u_\infty = 1$, $v_\infty = 0$, $p_\infty = -0.5$) are specified. For the upper and downstream boundaries the pressure is set to p_∞ and the velocity components are obtained by solving the momentum equations. On the lower boundary symmetry conditions are applied upstream and downstream of the plate. The no-slip conditions are imposed on the plate ($x = 1$ to $x = 2$). A wake flow develops downstream of the plate that diffuses slowly in the present case of laminar flow.

The finest grid used for the flat plate calculations consisted of 192×96 cells. In order to resolve the boundary layer on the plate the grid was clustered at $y = 0$ and stretched geometrically to $y = 1$ (see Fig. 2). For this grid the minimum spacing in the y direction is 0.002, and the stretching factor is 1.03. A series of nested coarse grids was obtained by coarsening the fine grids by a factor of two in each coordinate direction. In all cases shown below, the coarsest grid was 12×6 cells.

Line Gauss-Seidel relaxation was used for the computations. The complete relaxation process involves one sweep

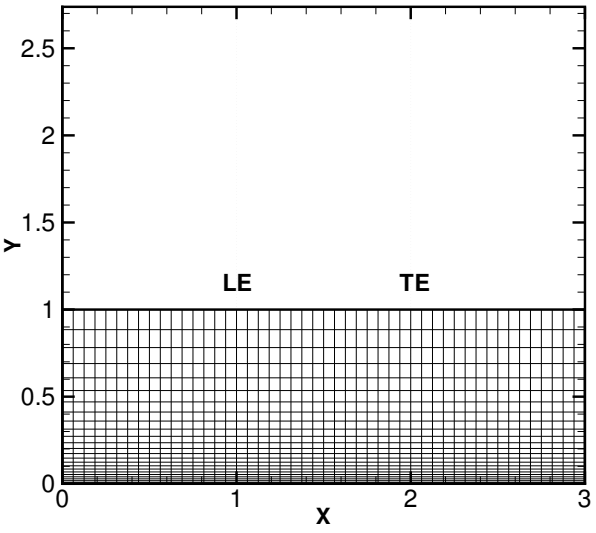

Fig. 2 Domain of flat plate flow with 48×24 cell grid.

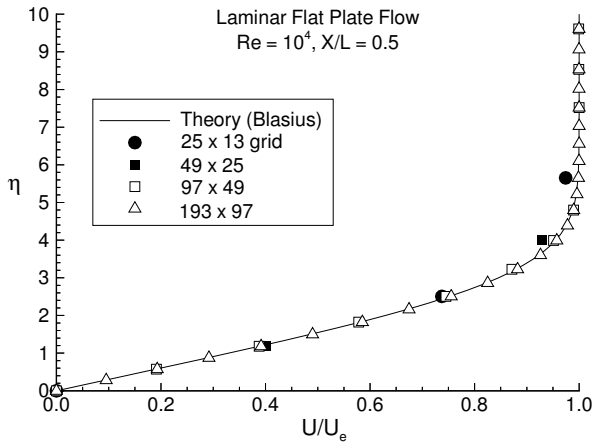

Fig. 3 Velocity profiles at midplate location for laminar flow over flat plate ($Re = 10,000$).

with vertical line solves and one sweep with horizontal line solves, along with some additional work near the plate. The relatively small amount of additional work is needed due to the coupling of the flow equations near the plate. Moreover, the points for $j \leq 3$ are relaxed with about three sweeps of horizontal solves. For the vertical line solves relaxation begins at the inflow boundary ($x = 0$) and proceeds to the outflow boundary ($x = 3$). In the case of the horizontal line solves relaxation starts at the outer boundary ($y = 1$) and continues to the inner boundary ($y = 0$). A $W(1,1)$ multigrid cycle was used; that is, one complete relaxation process was performed on each grid before restricting to the coarse grid, and one complete relaxation process was performed after the coarse-grid correction was added to the fine-grid solution.

The Reynolds number of the flow past the flat plate is 10,000. Figure 3 shows the variation of the velocity component u nondimensionalized by the boundary-layer

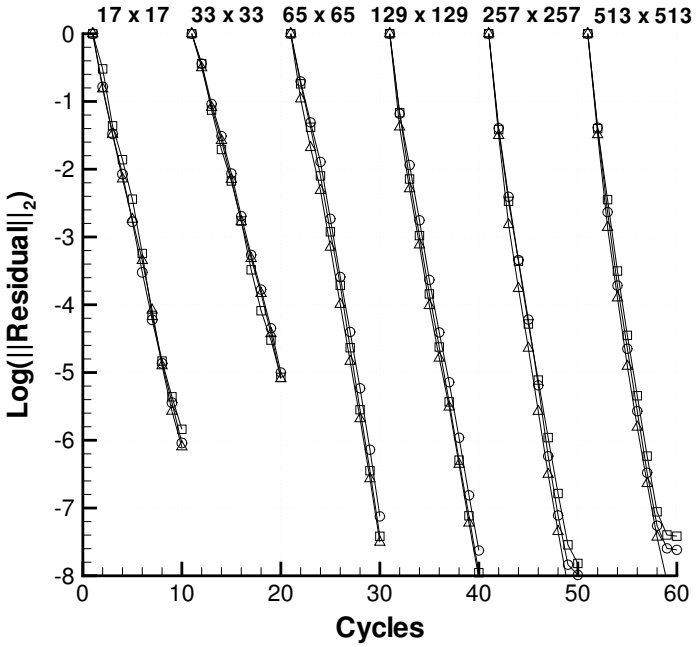

Fig. 4 Convergence behavior for laminar flow over flat plate ($Re = 10,000$). Open symbols for pressure residuals; closed symbols for x-momentum residuals.

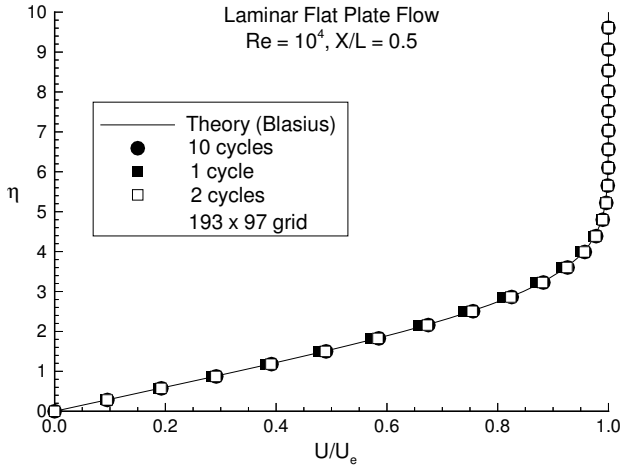

Fig. 5 Variation with multigrid cycles of velocity profile at midplate location for laminar flow over flat plate ($Re = 10,000$, 193×97 grid).

edge velocity (u_e) with the scaled normal coordinate η. The coordinate $\eta = 5y/\delta$, where δ is the thickness of the boundary layer. The computed velocity profiles are at the midplate location. Starting with the 96×48 cell grid, which has ten points in the boundary layer, there is excellent agreement with the classical Blasius solution. In Fig. 4 the convergence behavior of the scheme is shown. The L_2 norm of the residuals for the pressure and x-momentum equations is given for each $W(1,1)$ cycle. For most of the grids the residuals have been reduced more than 6 orders of magnitude in 10 cycles. The convergence rate on the finest

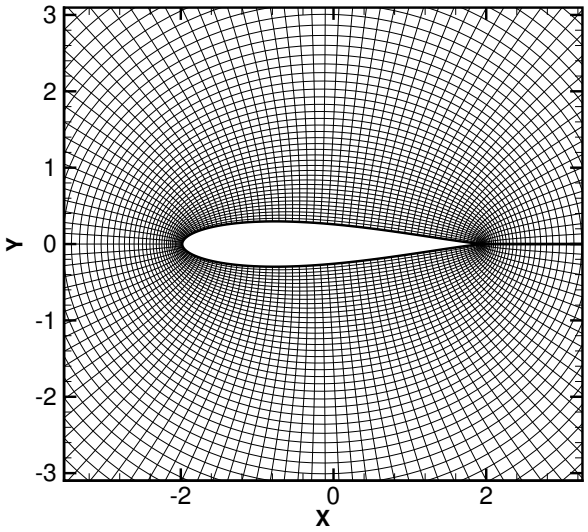

Fig. 6 Near field of 128 x 64 cell O-type grid for computing laminar flow over Kármán-Trefftz airfoil ($Re = 200$).

grid is 0.17 per cycle. As indicated in Fig. 5, the solution on the finest grid can nearly be obtained in a FMG process, involving only one multigrid cycle on each grid considered in Fig. 4.

Solutions were obtained for incompressible, viscous flow ($Re = 200$ based on chord) around a nonlifting Kármán-Trefftz airfoil. Previously, a form of the present numerical scheme was applied to inviscid airfoil flows, and an O-type mesh topology was used. So, initially in the present work, the same mesh topology was considered for viscous flows.

A Kármán-Trefftz airfoil was generated from a cylinder by a conformal mapping.[8] A trailing-edge angle of 10° is used, resulting in an airfoil of approximately 15% thickness. The airfoil flow is solved on a finite domain. At inflow points along the outer boundary the total pressure and flow inclination angle are specified. For outflow points the pressure is specified. The specified quantities are determined from the complex potential function for inviscid flow past the airfoil.

A fine grid for the airfoil calculation (512×256 cells) was constructed by generating an O-grid in the circle plane and mapping it to the airfoil plane. The near field of the 128×64 grid is displayed in Fig. 6. The outer boundary of the domain is roughly 3 chords from the airfoil. The coarsest grid in the grid sequence used for the multigrid solver contains 16×8 cells. On each grid a relaxation sweep started at the stagnation streamline, proceeded over the upper half of the domain, and then over the lower half of the domain. The relaxation sweep with radial solves was followed by sweeps with azimuthal solves near the airfoil, as in the flat plate case.

Convergence behavior in the FMG process for the airfoil calculations with the O-type mesh is shown in Fig. 7. On the finest grid the asymptotic convergence rate for the x-momentum and pressure equations is about 0.14 per cycle. There is somewhat slower convergence on the coarser meshes, with about five orders of magnitude reduction of

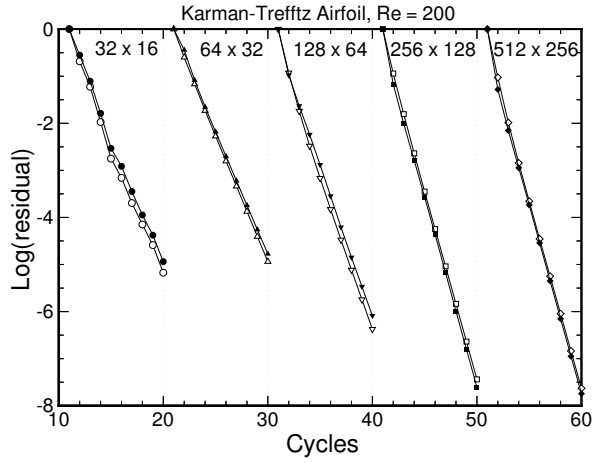

Fig. 7 Convergence behavior for laminar flow over nonlifting Kármán-Trefftz airfoil ($Re = 200$, O-type mesh topology). Open symbols for pressure residuals; closed symbols for x-momentum residuals.

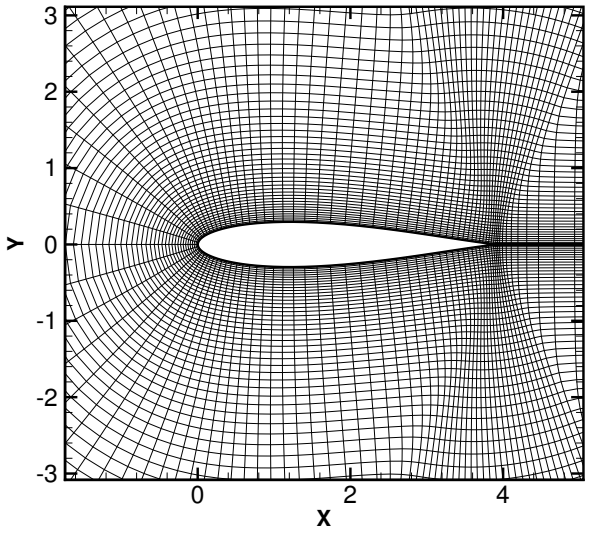

Fig. 8 Near field of 128 x 64 cell C-type grid for computing laminar flow over Kármán-Trefftz airfoil ($Re = 200$).

the residuals on the 64×32 cell grid. Such behavior was also observed by Roberts and Swanson[10] for inviscid flow.

To facilitate the resolution of the near and far wake regions, especially in the case of laminar flow where the mixing rate due to the physical diffusion is slow, a C-type mesh was generated for the airfoil calculations. A hyperbolic grid generator was used to create the mesh. The near field part of the grid is depicted in Fig. 8. In Fig. 9 the convergence histories for this mesh topology are presented. The average rate of reduction of the residual on the 512×256 grid is 0.19 for the pressure equation and 0.22 for the x-momentum equation. The slower rate for the x-momentum equation is surprising since the rate of convergence of the scheme should be dictated by the elliptic factor in this factorizable scheme. In addition, we do not observe this behavior with O-type mesh computation.

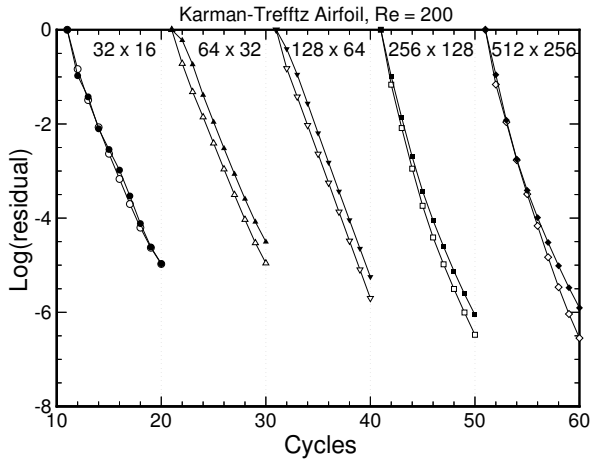

Fig. 9 Convergence behavior for laminar flow over nonlifting Kármán-Trefftz airfoil ($Re = 200$, C-type mesh topology). Open symbols for pressure residuals; closed symbols for x-momentum residuals.

In order to estimate the work required by the present and R-K schemes, we consider an operation count based on residual evaluations and the the number of cycles to achieve a specific reduction in residuals. For a W(m, n) multigrid cycle, there are $m+n$ residual evaluations on the fine grid. The restriction operator requires a residual calculation on the fine grid and one on the next coarser grid, with work corresponding to 1/4 that on the fine grid. In this assessment we neglect the cost of interpolating the residuals and solutions between the grid levels. For a W(m, n) cycle, we have that[9]

$$\frac{\text{WU}}{W\text{–cycle}} \approx (m+n+1+\frac{1}{4})(1+\frac{1}{2}+\frac{1}{4}+\cdots)$$
$$= 2(m+n+\frac{5}{4}),$$

where WU means work unit. The WU per cycle for the current scheme with a W(2,1) cycle with only radial relaxation sweeps (neglecting additional work at surface boundary with azimuthal solves) is 8.5. With the five-stage R-K scheme and a W(1,0) cycle, the WU per cycle is 12.5.

With the present scheme an additional residual evaluation is incurred due to the Gauss-Seidel updating of the solution. If we include that, the ratio of residual evaluations for the present scheme to that of the R-K scheme would be increased to 10.5 for the W(2,1) cycle used on the C-type grid and 8.5 for the W(1,1) cycle used for the O-type grid. Since we fully expect to have about the same number of residual evaluations for the different mesh topologies, the estimate of WU per cycle required by the present scheme is not altered.

For the two schemes there is a difference in computational effort resulting from scalar tridiagonal and pentadiagonal inversions. As indicated previously each relaxation sweep of the present scheme requires one tridiagonal solve and two pentadiagonal solves (corresponding to the three flow equations) for the grid lines not in the direction of the relaxation. Since the operation count for a pentadiagonal inversion is about two times that for a tridiagonal inversion,

the work required on the fine grid with $m+n=3$ is roughly proportional to that for 15 tridiagonal solves. For the R-K scheme there is a scalar tridiagonal inversion for each flow equation, each coordinate direction, and each of the five stages due to the residual smoothing procedure used to extend stability. So, in the particular case of three flow equations, the work due to this part of the scheme is proportional to 30 tridiagonal solves. Thus, the R-K scheme considered here[12] requires about two times as much work as the present scheme due to inversions. It should also be pointed out that the R-K scheme used here is a (5,3) scheme, which means that the complete residual, including viscous and numerical dissipation terms, is evaluated only on three stages.

In order to roughly estimate the total speedup (i.e., product of WU per cycle and number of cycles for desired level of convergence) of the present scheme relative to the R-K scheme, we not only consider residual reduction for the x-momentum equation but also the convergence of the drag coefficient (C_d). For a residual reduction of four orders of magnitude, the present scheme is at least an order magnitude faster than the R-K scheme for the laminar airfoil flow. This speedup is also evident in Figs. 10 and 11, which show the variation of C_d with multigrid cycles for the two schemes. The speedup of the present scheme on the finer meshes (mesh density $\geq 256 \times 128$ cells) can exceed a factor of 25.

Pressure and velocity contours for the solution on the 512×256 C-type grid are depicted in Figs. 12 and 13. The thickness of the attached boundary layer is about 0.25 airfoil chords, and there are about 70 points in the boundary layer at the midchord location. Slow diffusion of the airfoil wake is evident. In Figs. 14 and 15 the pressure and skin friction computed with the present scheme on various grid densities are compared with the fine grid results obtained with the R-K scheme (where the free-stream Mach number was set to 0.1). There is generally very good agreement starting with the 128×64 grid.

Concluding Remarks

A multigrid algorithm with essentially $O(N)$ behavior has been developed for the steady Navier-Stokes equations. It has the virtue of simplicity; conventional finite-difference or finite-volume discretizations of the governing equations may be used, allowing flexibility in the choice of the underlying numerical method. Appropriate discretization and efficient treatment of the pressure boundary condition has been demonstrated. Solutions have been obtained for laminar flow past a flat plate with essentially texbook multigrid efficiency. Furthermore, the multigrid method has been used to solve viscous flow with curvature effects. Fast convergence was obtained for this case also. With the present scheme more than an order of magnitude reduction in computational effort has been achieved when compared with a R-K based multigrid scheme.

Further studies of the present scheme are required to determine the effects of mesh aspect ratio and grid stretching on convergence rate, and thus, on the discrete factorizability of the algorithm. While significant gains in computational efficiency have been achieved for laminar flow, much greater gains (i.e., two orders of magnitude) are anticipated with the extension of factoriazable schemes to allow computation of turbulent flows.

Acknowledgments

The author would like to thank Dr. David Sidilkover and Dr. Thomas Roberts for helpful discussions and suggestions. In addition, the author would like to thank Dr. James Thomas for his encouragement and for fostering the environment in which this work has been carried out.

References

[1] Jameson, A., "Solution of the Euler Equations for Two Dimensional Transonic Flow by a Multigrid Method," *Appl. Math. Comput.*, vol. 13, nos. 3 and 4, pp. 327–355, 1983.

[2] Mulder, W., "Multigrid Relaxation for the Euler Equations," *J. Comput. Phys.*, vol. 60, no. 2, pp. 235–252, 1985.

[3] Anderson, W. K., Thomas, J. L., and Whitfield, D. L., "Three-Dimensional Multigrid Algorithms for the Flux-Split Euler Equations," NASA Technical Paper 2829, 1988.

[4] Warren, G. P., and Roberts, T. W., "Multigrid Properties of Upwind-Biased Data Reconstructions," *Sixth Copper Mountain Conference on Multigrid Methods,* NASA Conference Publication 3224, Part 2, 1993.

[5] Brandt, A., "Multigrid Techniques: 1984 Guide with Applications to Fluid Dynamics," GMD-Studie 85, GMD-FIT, 1985.

[6] Brandt, A., and Yavneh, I., "Accelerated Multigrid Convergence and High-Reynolds Recirculating Flows," *SIAM J. Sci. Statist. Comput.*, vol. 14, no. 3, pp. 607–626, 1993.

[7] Thomas, J. L., Diskin, B., and Brandt, A., "Distributed Relaxation Multigrid and Defect Correction Applied to the Compressible Navier-Stokes Equations." *AIAA Paper* 99-3334, 14th Computational Fluid Dynamics Conference, Norfolk, VA, July 1999.

[8] Roberts, T. W., Sidilkover, D., and Swanson, R. C., "Textbook Multigrid Efficiency for the Steady Euler Equations," *AIAA Paper* 97-1949, 1997.

[9] Roberts, T. W., Swanson, R. C., and Sidilkover, D., "An Algorithm for Ideal Multigrid Convergence for the Steady Euler Equations," *Computers and Fluids*, vol. 28, nos. 4–5, pp. 427–442, 1999.

[10] Roberts, T. W., and Swanson, R. C., "Extending Ideal Converging Multigrid Methods to Airfoil Flows," *AIAA Paper* 99-3337, 1999.

[11] Sidilkover, D., and Ascher, U. M., "A Multigrid Solver for the Steady State Navier-Stokes Equations using the Pressure-Poisson Formulation," *Comp. Appl. Math.* vol. 14, no. 1, pp. 21–35, 1995.

[12] Swanson, R. C., and Turkel, E., "Multistage Schemes with Multigrid for Euler and Navier-Stokes Equations - Components and Analysis," *NASA TP* 3631, August 1997.

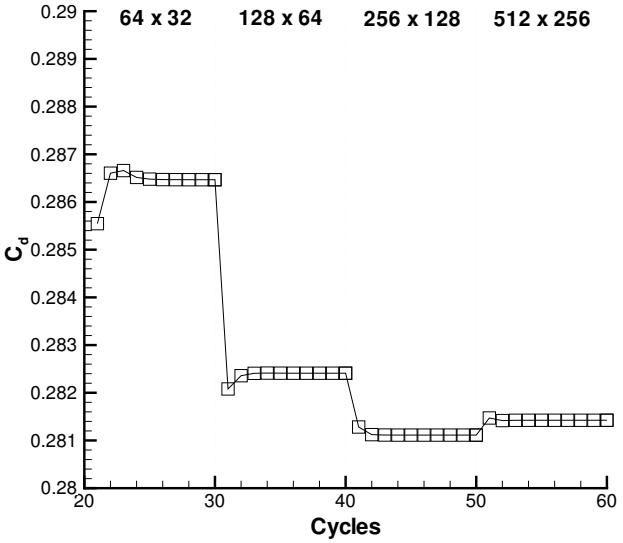

Fig. 10 Convergence history of total drag for laminar flow over nonlifting Kármán-Trefftz airfoil ($Re = 200$).

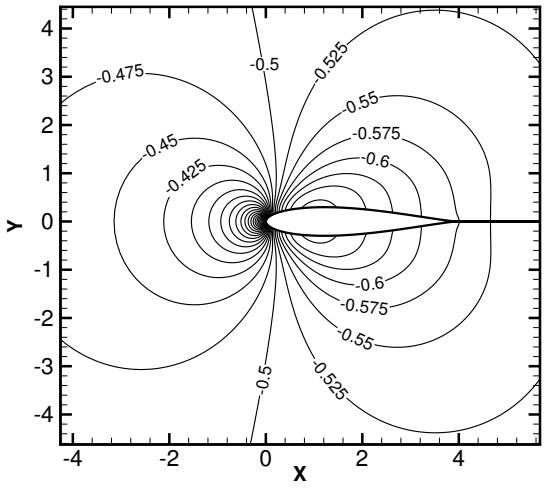

Fig. 12 Pressure contours for laminar flow over nonlifting Kármán-Trefftz airfoil ($Re = 200$).

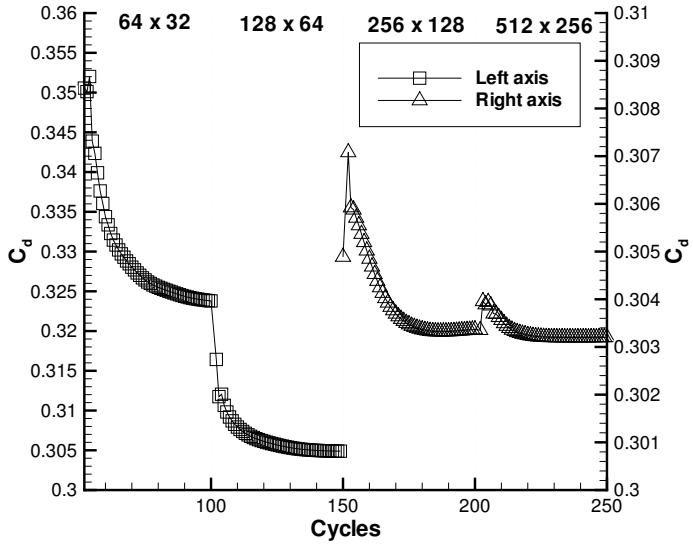

Fig. 11 Convergence history with R-K scheme of total drag for laminar flow over nonlifting Kármán-Trefftz airfoil ($Re = 200$).

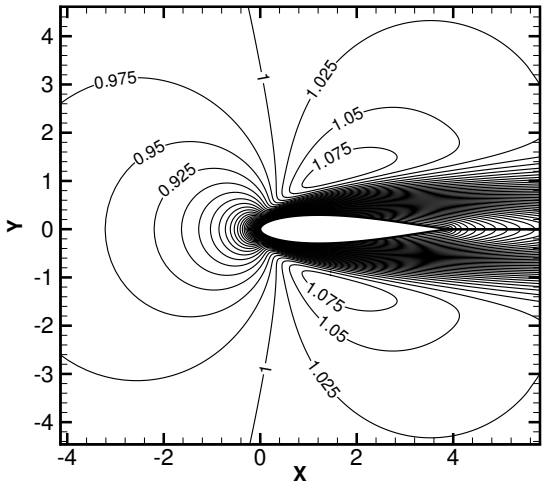

Fig. 13 Velocity contours for laminar flow over nonlifting Kármán-Trefftz airfoil ($Re = 200$).

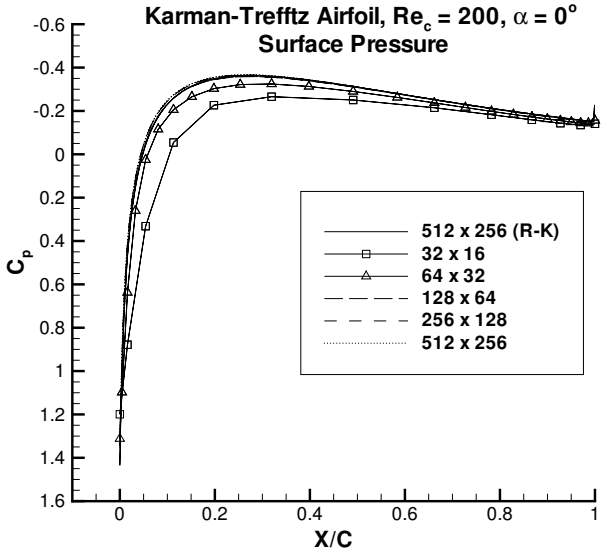

Fig. 14 Surface pressure distribution for laminar flow over nonlifting Kármán-Trefftz airfoil (Re = 200).

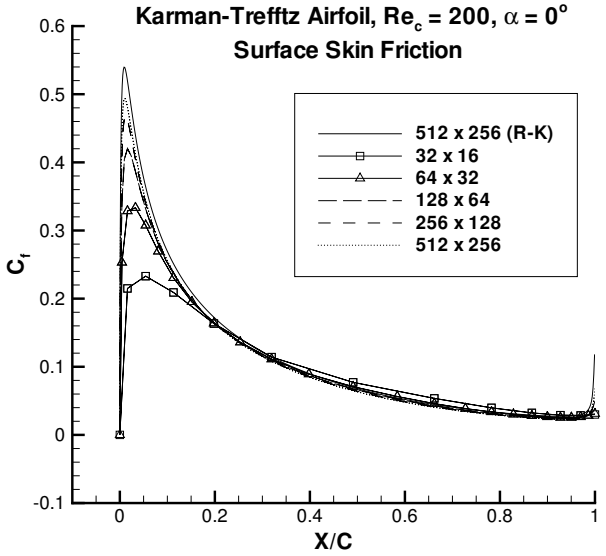

Fig. 15 Surface skin-friction distribution for laminar flow over nonlifting Kármán-Trefftz airfoil ($Re = 200$).